Available online at www.sciencedirect.com

SciVerse ScienceDirect

Ceramics International 39 (2013) 4133–4138

CERAMICS INTERNATIONAL

www.elsevier.com/locate/ceramint

Effects of pH on the microstructures and optical property of $FeWO_4$ nanocrystallites prepared via hydrothermal method

Fang Yu*, Liyun Cao, Jianfeng Huang, Jianpeng Wu

Key Laboratory of Auxiliary Chemistry and Technology for Light Chemical Industry, Ministry of Education, Shaanxi University of Science and Technology, Xi'an 710021, China

Received 10 October 2012; received in revised form 31 October 2012; accepted 31 October 2012
Available online 16 November 2012

Abstract

$FeWO_4$ nanocrystallites were prepared via a hydrothermal process using ferrous ammonium sulfate [$(NH_4)_2Fe(SO_4)_2 \cdot 6H_2O$] and sodium tungstate [$Na_2WO_4 \cdot 2H_2O$] as raw materials. The as-prepared nanocrystallites were characterized by X-ray diffraction(XRD), Scanning Electron Microscopy (SEM), Transmission Electron Microscopy (TEM), and UV–vis analyses. Results show that pH values significantly influence the phase and morphology of the as-prepared $FeWO_4$ nanocrystallites. It is easy to obtain pure $FeWO_4$ nanocrystallites in a wide range of the pH = 2–11. The powders display a hexagonal flakes morphology under acidic conditions of pH = 2. With the increase of pH, the morphology change from hexagonal flakes into rods. By UV–vis analysis, the optical band gap of the $FeWO_4$ powders is calculated to be about 2.40 eV.

Keywords: $FeWO_4$; Hydrothermal method; Optical property

1. Introduction

Metal tungstates have been of practical interest for a long time due to their luminescence behavior and structural properties [1]. One of them, monoclinic ferrous tungstate ($FeWO_4$) have highly potential and technological applications in many areas, such as scintillation detectors, optical fibers, humidity sensors, photoanodes, phase-change optical recording devices, laser hosts, catalysts, pigments, etc. [2–7]. In addition, with the development of science and technology, the nano-structured materials have attracted much more attention compared with their bulk materials [8]. Thus, the synthesis of well-crystallized $FeWO_4$ crystallites, especially $FeWO_4$ nano-particles, has recently drawn increasing attention. Diverse techniques have been developed to synthesize $FeWO_4$ powders, ranging from the conventional solid-state reaction method at high temperature, wet chemical method such as co-precipitation [9], the polymeric precursor method and the hydrothermal/solvothermal method [10,11], to the spray pyrolysis method [12]. The conventional solid-state reaction method consumes large energy due to high reaction temperature and repeated calcining–crushing cycles, and $FeWO_4$ particles prepared by this method are always relatively large in particle size with irregular morphology and impure in chemical composition. Though well-blending reacting constituents on atomic level can be realized effectively in aqueous solutions, the precipitate and the polymeric precursors obtained are still further calcined at relatively high temperatures to remove organic materials. Hydrothermal method emerged as useful tool for the fabrication of microcrystallite $FeWO_4$ nano-materials with advantages such as low synthesis temperature and controllable particle size [13].

Herein, in the present study, a hydrothermal method was employed for the preparation of $FeWO_4$ nano-particles with perfectly crystalline morphology at low temperature, and the effects of pH values on the crystallization and development of $FeWO_4$ crystallites were investigated. The as-prepared $FeWO_4$ nano-particles exhibited excellent optical properties. To the best of our knowledge, no such

*Corresponding author. Tel./fax: +86 29 86168803.
E-mail address: yufang8642@163.com (F. Yu).

0272-8842/$ - see front matter © 2012 Elsevier Ltd and Techna Group S.r.l. All rights reserved.
http://dx.doi.org/10.1016/j.ceramint.2012.10.269

studies have ever been reported, and it is indeed a good preparing method because of its simple instrumentation, easy manipulation and low synthetic temperature.

2. Experimental

2.1. Synthesis of $FeWO_4$ powders

All the reagents used in present experiments were of analytical purity and used as received without further purification. The experimental procedure for preparing $FeWO_4$ powders was as follows: ferrous ammonium sulfate $[(NH_4)_2Fe(SO_4)_2 \cdot 6H_2O]$ (3 mmol) and sodium tungstate $[Na_2WO_4 \cdot 2H_2O]$ (3 mmol) were each dissolved in 5 mL of distilled water. First, the $Na_2WO_4 \cdot 2H_2O$ solution was added dropwise to the $[(NH_4)_2Fe(SO_4)_2 \cdot 6H_2O]$ solution with magnetic stirring. Afterwards, the pH of the precursor suspension was adjusted to 1, 2, 3, 4, 6, 7, 9, 10, 11 and 12 by addition of either dilute hydrochloric acid or sodium hydroxide solution. Finally, the pH-adjusted precursor suspension was transferred into a Teflon-lined stainless steel autoclave with a filling capacity of 60% and maintained in an oven at 190 °C for 24 h. After the hydrothermal system cooled down naturally to room temperature, the final products were collected, washed repeatedly with distilled water, filtered off, and dried at 60 °C for 4 h.

2.2. Characterization

The phase structure and phase purity of the as-synthesized products were examined by X-ray diffraction (XRD), using a D/MAX-2200PC instrument, with the X-ray diffractometer using Cu-Kα radiation ($\lambda = 0.15406$ nm) at a scan rate of $8^\circ\ min^{-1}$ (Rigaku, Japan). The microstructures of the powders were observed with SEM (JSM-6390A) and TEM (JEM-3010). UV–vis diffuse reflectance spectra (DRS) of the $FeWO_4$ powders were measured at room temperature with a Lambda 950 spectrophotometer.

3. Results and discussion

3.1. XRD analyses

The XRD patterns of the as-synthesized powders with different pH values at 190 °C for 24 h are shown in Fig. 1. The pH of the precursor medium has a crucial effect on the formation of tungstate phase in the hydrothermal process. Clearly, when the pH of the mixed dispersion was lowered to 2, the product was mainly WO_3, when the pH was increased to 12, the product was mainly Fe_3O_4. When pH was 2–11, all diffraction peaks were readily indexed as the monoclinic phase of $FeWO_4$ with unit cell parameters of $a = 4.753$ Å, $b = 5.720$ Å, $c = 4.968$ Å, $\beta = 90^\circ$ and a space group of P2/c, which was in good agreement with the literature values (JCPDS Card file no.74-1130). The strong and sharp diffraction peaks indicated that the obtained products were well crystallized.

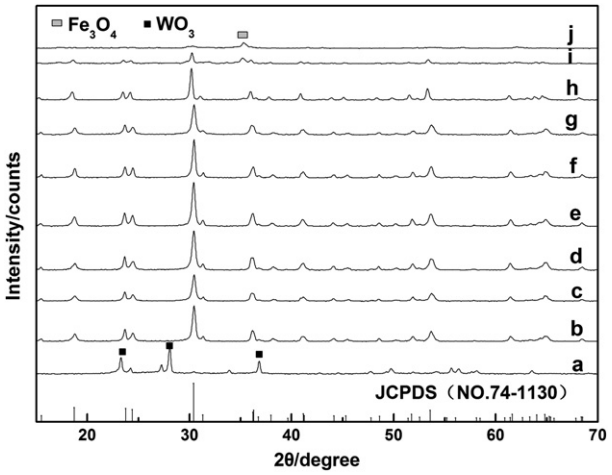

Fig. 1. XRD patterns of as-prepared $FeWO_4$ nanopowders with different pH values: (a) pH = 1; (b) pH = 2; (c) pH = 3; (d) pH = 4; (e) pH = 6; (f) pH = 7; (g) pH = 9; (h) pH = 10; (i) pH = 11 and (j) pH = 12.

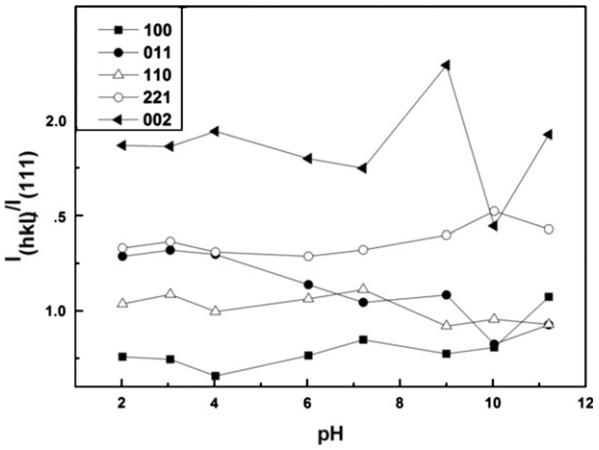

Fig. 2. Relative intensity of as-prepared $FeWO_4$ nanocrystallites' planes changed with pH values.

Fig. 2 shows the relative intensity ($I_{(hkl)}/I_{(111)}$) [14] of as-prepared $FeWO_4$ nanocrystallites' planes changed with pH values according to the XRD data. As shown in Fig. 2. The relative intensity of (002) and (011) planes' diffraction peak for the strongest (111) planes' diffraction peak changed rigidly with different pH values. The relative intensity of the (002) planes shows the N-type changes (increase first and decreases then increase again) at pH = 7–11, the relative intensity of the (011) planes shows the V-type changes (decrease first then increase again) at pH = 9–11, and its relative intensity is higher than calculated $FeWO_4$ standard card's relative intensity of 0.175 (JCPDS no. 74-1130), indicating that $FeWO_4$ crystallite prepared in the range of pH = 7–11 along the (002) and (011) planes has a clear preferential orientation with the changes in pH. Taking all these factors, we can conclude that the pH value would denote a change in the morphology.

3.2. Morphologies of the resulting crystallites

Fig. 3 shows the SEM images of the as-prepared $FeWO_4$ powders with different pH values. Clearly, the pH of the

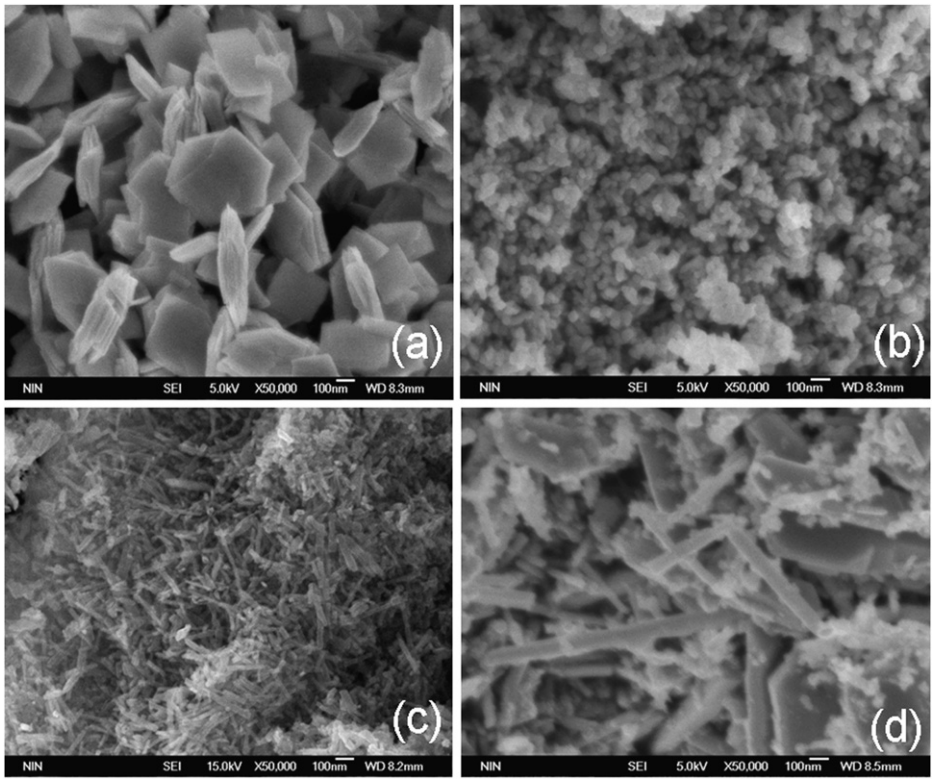

Fig. 3. SEM images of as-prepared $FeWO_4$ nanopowders with different pH values: (a) pH=2; (b) pH=7; (c) pH=9 and (d) pH=10.

precursor medium has a crucial effect on its morphology in the hydrothermal process. Controlled experiments were carried out to investigate the influence of pH on the phase evolution of $FeWO_4$. The powders display a hexagonal flakes morphology under acidic conditions of pH=2 with a uniform grain size of 200–400 nm (Fig. 3a). With the increase of pH in the neutral conditions (pH=7), the powder grain size decreases, and at the same time, the morphology changes from hexagonal flakes into tiny nanoparticles (Fig. 3b). Increasing the pH to 9, the morphology changes from tiny nanoparticles into thin rods (Fig. 3c). Further increasing the pH to 10, the rods' diameter significantly increased with the pH, along with the small amount of flakes and granular $FeWO_4$ nanocrystallite (Fig. 3d).

Fig. 4 displays a representative TEM image of the as-synthesized $FeWO_4$ powders with different pH values. High-magnification TEM image shows that the powders have an average grain size of 200–400 nm under acidic conditions of pH=2, which is in agreement with the SEM observation. As shown in Fig. 4a, the corresponding SAED pattern taken from the selected part, which is very sharp, indicates that the product is highly crystalline. With the pH increases to neutral condition (pH=7), high-magnification TEM image shows that the nanorods' tiny nanoparticles' grain size was decreased to 100 nm. As shown in Fig. 4b, the corresponding SAED pattern taken from the selected part, which is very sharp, indicates that the product is highly crystalline. The clearly visible (002) and (021) lattice planes of the $FeWO_4$ phase confirm the long-range order crystallization of the powders. When the pH increased to 9, high-magnification TEM image shows that the nanorods have an average diameter of 30–40 nm and lengths in the range 300–400 nm, which is in agreement with the SEM observation. HRTEM image of an individual nanorod and the clear lattice fringes also demonstrate its single-crystalline nature. The observed lattice spacing of 2.58 Å in Fig. 4c correspond to the (002) planes of the monoclinic $FeWO_4$, indicating that $FeWO_4$ crystallite has a clear preferential orientation along the (002) planes, which is consistent with the results of the analysis of Fig. 2. Further increasing the pH to 10, the rods' diameter significantly increased to 70–100 nm, and lengths was increased to 400–600 nm. The lattice fringes are measured as about 5.57 Å and 4.83 Å, which correspond to the (010) and (100) planes of the monoclinic phase $FeWO_4$ respectively, the regularly arranged spots showing that the it is single $FeWO_4$ nanocrystallite. with the changes in pH.

3.3. Formation mechanism of the morphologies of $FeWO_4$

On the basis of the experimental results and observations, the possible reactions carried out are proposed as follows:

$$4(NH_4)_2Fe(SO_4)_2 \rightarrow 8NH_4^+ + 4Fe^{2+} + 8SO_4^{2-} \quad \text{(a)}$$

$$4Fe^{2+} + O_2 + (4+2x)\ H_2O \leftrightharpoons 2Fe_2O_3 \cdot xH_2O + 8H^+ \quad \text{(b)}$$

$$8NH_4^+ + 8H_2O \rightarrow 8NH_3 \cdot H_2O + 8H^+ \quad \text{(c)}$$

$$Na_2WO_4 \rightarrow 2Na^+ + WO_4^{2-} \quad \text{(d)}$$

$$Fe^{2+} + WO_4^{2-} \rightarrow FeWO_4 \quad \text{(e)}$$

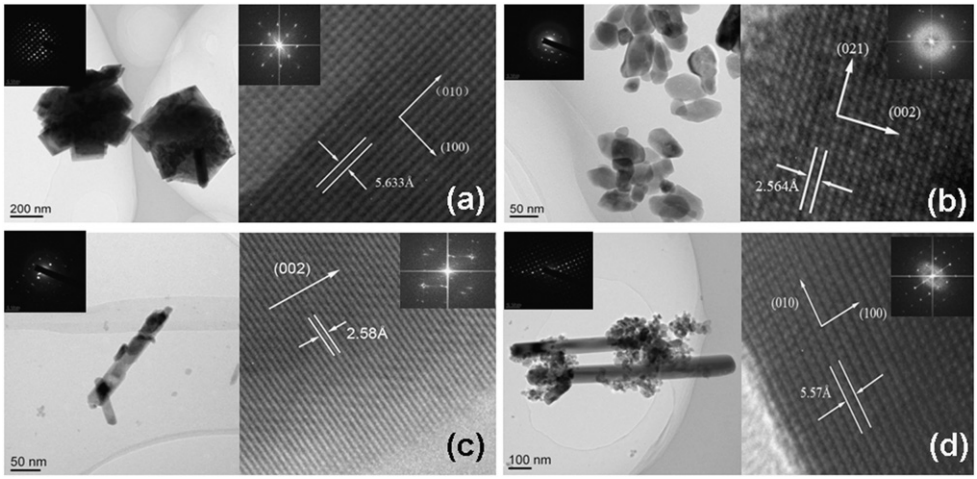

Fig. 4. TEM images of as-prepared $FeWO_4$ nanopowders with different pH values: (a) pH=2; (b) pH=7; (c) pH=9 and (d) pH=10.

Table 1
Influence of pH on formation of phase and shape of as-prepared $FeWO_4$ nanocrystallites.

pH	Diameter (nm)	Length (nm)	Morphology	Phase
2	300–400	30–40	Hexagonal flakes	amorphous, $FeWO_4$
7	40–70	70–100	Tiny nanoparticles	amorphous, $FeWO_4$
9	30–40	300–400	Thin rods	amorphous, $FeWO_4$
10	70–100	400–600	Rods, flakes and tiny nanoparticles	amorphous, $FeWO_4$

$$WO_4^{2-} + 2H^+ \rightarrow WO_3 \cdot nH_2O \quad (f)$$

$$Fe^{2+} + 3OH^- \rightarrow 2NH_3 + Fe(OH)_2 + 2SO_4^{2-} + 2H_2O \quad (j)$$

$$4Fe(OH)_2 + O_2 + 2H_2O \rightarrow 4\ Fe(OH)_3 \quad (h)$$

$$2Fe(OH)_3 \rightarrow Fe_2O_3 + 3H_2O \quad (i)$$

$$Fe^{2+} + Fe^{3+} + 4H_2O \leftrightharpoons Fe_3O_4 + 4H^+ \quad (g)$$

$(NH_4)_2Fe(SO_4)_2$ is typically used as the Fe source in the preparation of $FeWO_4$ by the hydrothermal method. As shown in Reaction (a), Fe^{2+} will be produced when $(NH_4)_2Fe(SO_4)_2$ was ionized, some Fe^{2+} would be oxidized to Fe_2O_3 in the air (Reaction (b)), but Fe^{2+} exists steadily for H^+ inhibiting the reaction equilibrium shifting right by hydrolysis of NH_4^+ (Reaction (c)), and WO_4^{2-} will be produced when Na_2WO_4 dissolves in water (Reaction (d)). When these two solutions are mixed, a black precipitate of $FeWO_4$ will immediately be produced in the range of pH=2–10 (Reaction (e)). Introducing too much HCl will lead to the generation of tungsten oxide hydrates ($WO_3 \cdot nH_2O$) when is pH < 2 (Reaction (f)), while introducing too much NaOH will accelerate the reaction (Reactions (b) and (g)) equilibrium to shift to the right, so ferroferric oxide (Fe_3O_4) was formed when was pH > 10 (Reactions (j),(h), (i) and (g)).

The influence of pH on the formation of phase and shape of as-prepared $FeWO_4$ nanocrystallites is shown in Table 1, and the phase and morphology evolution for $FeWO_4$ is shown in Fig. 5. It is worthy to note that hexagonal flakes

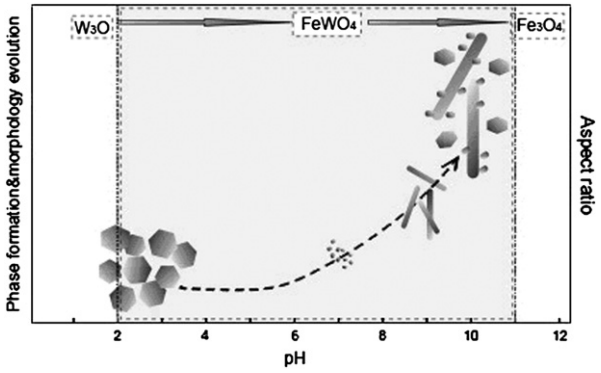

Fig. 5. A map of the phase and morphology evolution for $FeWO_4$ by the hydrothermal method.

morphology under acidic conditions of pH=2 is clearly associated with the crystalline growth along the (010) and (100) planes, while the preparation of $FeWO_4$ nanorods with NaOH at pH=9 leads to the extinction of (0 0 2) diffraction line notably. The above morphology evolution for $FeWO_4$ can be understood from the view-point of the intrinsic structures of the tungstates. The alternative infinite chain structures can be clearly seen from the molecule modeling results, as shown in Fig. 6 [4]. In particular, the special feature of the (100) face is that the ordered $[WO_4^{2-}]$ chain that lies on the (100) face and all the negative ordered $[WO_4^{2-}]$ anion are exposed, while all the positive Fe^{2+} ion are shielded. H^+ was produced as a result of introducing HCl; the attraction between positive and

negative charges inhibit the growth of (100) face. This could be the reason why the powders display a hexagonal flakes morphology under acidic conditions of pH=2. The similar special, structural features of the (100) face in the wolframite structure could shed some light on the high intrinsic growth habits such as those observed in various tungstate systems [15]. The (100) faces contain units fully composed of highly distorted octahedral-Fe chain which was shielded by the chains of octahedral-W, the same as (0 0 1) and (0 0 2) faces. For the pH increase to 9, the repelling interaction between OH^- and $[WO_4^{2-}]$ anion plays a key role in the highly intrinsic preferential growth along the (0 0 2) faces of the $FeWO_4$ crystals.

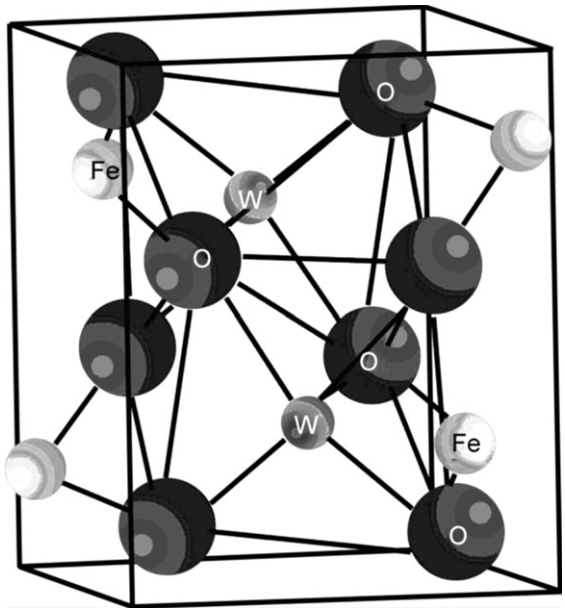

Fig. 6. Crystal structure of iron tungstate.

3.4. Optical properties

Fig. 7 shows the ultraviolet–visible diffuse reflectance spectrum of the as-prepared $FeWO_4$ powders with different pH values. The absorption edge of the sample extended nearly to the whole spectra of visible light, which implies the possibility of high photocatalytic activity of these materials under the visible light irradiation.

The spectrum shows a absorptions at 300–600 nm. The band gap of the as-synthesized $FeWO_4$ was calculated by the following equation [12,16]:

$$\alpha h\nu = \left(h\nu - E_g\right)^n$$

where α is the absorbance, h is the Planck constant, v is the photon frequency, E_g is the energy gap, and n is the pure numbers associated with the different types of electronic transitions. For $n=1/2$, 2, 3/2, and 3, the transitions are the direct allowed, indirect allowed, direct forbidden, and

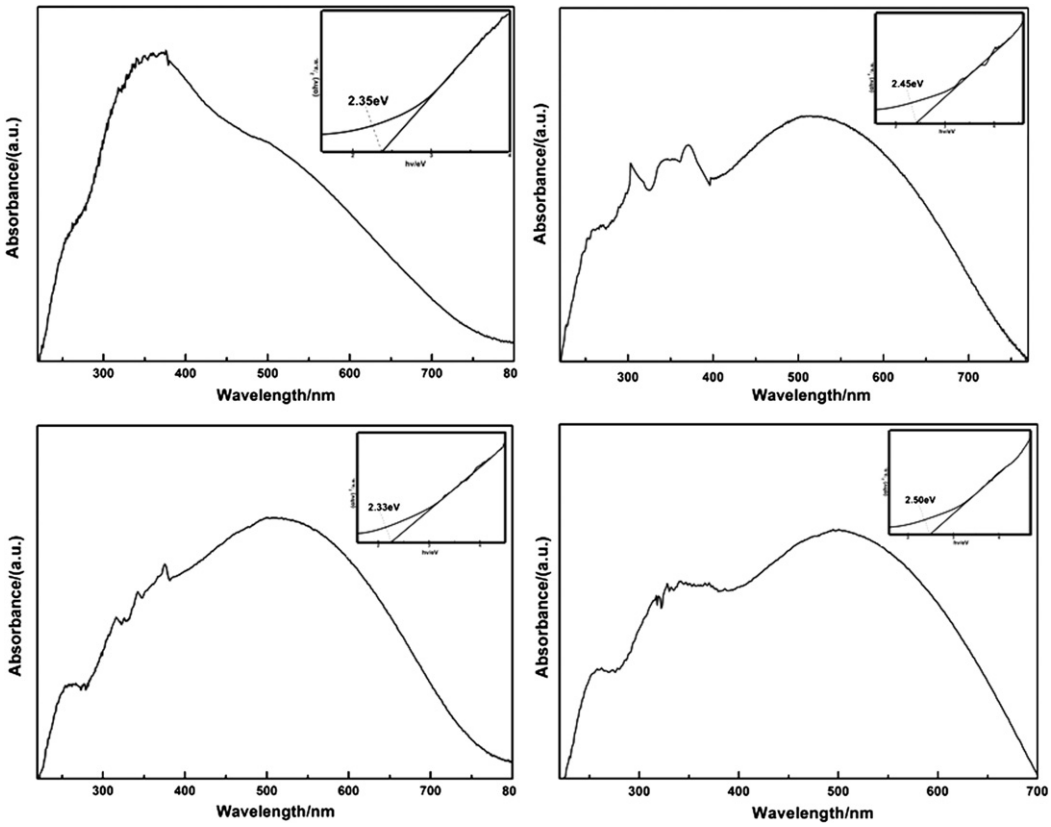

Fig. 7. UV–vis diffuse spectrum and the relationship between $(\alpha h\nu)^2$ and $h\nu$ of the as-prepared $FeWO_4$ powders under different pH values: (a) pH=2; (b) pH=7; (c) pH=9 and (d) pH=10.

indirect forbidden, respectively. The value of n for $FeWO_4$ equals to 1/2 and its band gap is estimated ($\alpha = 0$) to be 2.35 eV, 2.45 eV, 2.33 eV and 2.5 eV when pH values are 2, 7, 9 and 10 respectively (shown in inset of Fig. 7), which is little greater than the reported values (ca. 2.0 eV) of bulk crystals [17]. The prepared powders exhibit a blue-shift phenomenon, possibly due to the quantum size effect of the prepared nanopowders. We recognized that the morphology and grain size of $FeWO_4$ played a role in increasing the energy band gap.

Therefore, the energy of the band gap could be estimated to be about 2.40 eV for $FeWO_4$ powders. This indicates that the nanosized $FeWO_4$ has a suitable band gap for photocatalytic decomposition of organic contaminants under visible light irradiation.

4. Conclusion

In summary, the pure $FeWO_4$ nanopowders were prepared using a hydrothermal method. Results show that pH values significantly influence the phase and morphology of as-prepared $FeWO_4$ nanocrystallites. It is easy to obtain pure $FeWO_4$ nanocrystallites in a wide range of the pH = 2–11. The powders display a hexagonal flakes morphology under the acidic conditions of pH = 2. With the increase of pH, the morphology change from hexagonal flakes into rods. By UV–vis analyses, the optical band gap of the $FeWO_4$ powders is calculated to be 2.40 eV, indicating that the nanosized $FeWO_4$ has a suitable band gap for photocatalytic decomposition of organic contaminants under visible light irradiation.

Acknowledgments

This work was supported by National Natural Science Foundation of China (50962047), Special fund of the Education Department of Shaanxi Province Natural Science (no. 11JK0820), Special fund of the Education Department of Shaanxi Province Natural Science (no. 2010JK444), Special fund of the Education Department of Shaanxi Province Natural Science (no. 09JK361).

References

[1] Hong-Wei Liao, Yan-Fei Wang, Xian-Min Liu, Ya-Dong Li, Yi-Tai Qian, Hydrothermal preparation and characterization of luminescent $CdWO_4$ nanorods, Chemistry of Materials 12 (2000) 2819–2821.

[2] H. Grassmann, H.-G. Moser, E. Lorenz, Scintillation properties of $ZnWO_4$, Journal of Luminescence 33 (1985) 109–113.

[3] F.D. Hong Wang, D.D. Medina, Liu, Ya-Dong Zhous, The line shape and zero-phonon line of the luminescence spectrum from zinc tungstate single crystals, Journal of Physics: Condensed Matter 6 (1994) 5373–5386.

[4] S. Rajagopal, V.L. Bekenev, D. Nataraj, O.Yu Khyzhun, Electronic structure of $FeWO_4$ and $CoWO_4$ tungstates: first-principles FP-LAPW calculations and X-ray spectroscopy studies, Journal of Alloys and Compounds 496 (2010) 61–68.

[5] Qiao Zhang, Wei-Tang Yao, Xianyu Chen, Liwei Zhu, Yibing Fu, Guobin Zhang, Liusi Sheng, Shu-Hong Yu, Nearly monodisperse tungstate MWO_4 microspheres (M = Pb, Ca):surfactant-assisted solution synthesis and optical properties, Crystal Growth and Design 7 (2007) 1423–1431.

[6] Ruigen Chen, Jinhong Bi, Ling Wu, Wanjun Wang, Zhaohui Li, Xianzhi Fu, Template-free hydrothermal synthesis and photocatalytic performances of novel Bi_2SiO_5 nanosheets, Inorganic Chemistry 48 (2009) 9072–9076.

[7] Purnendu Parhi, T.N. Karthik, V. Manivannan, Synthesis and characterization of metal tungstates by novel solid-state metathetic approach, Journal of Alloys and Compounds 465 (2008) 380–386.

[8] Ye Gao, Jingzhe Zhao, Yanchao Zhu, Shanshan Ma, Xiaodan Su, Zichen Wang, Wet chemical process of rod-like tungsten nanopowders with iron (II) as reductive agent, Materials Letters 60 (2006) 3903–3905.

[9] V. Vinothini, Paramanand Singh, M. Balasubramanian, Synthesis of barium titanate nanopowder using polymeric precursor method, Ceramics International 32 (2006) 99–103.

[10] Zhen Liang, Wen-Shou Wang, Cheng-Yan Xu, Wen-Zhu Shao, Lu-Chang Qin, A facile hydrothermal route to the large-scale synthesis of $CoWO_4$ nanorods, Materials Letters 62 (2008) 1740–1742.

[11] Song Zuwei, Ma Junfeng, Sun Huyuan, Sun Yong, Fang Jingrui, Liu Zhengsen, Gao Chang, Ye Liu, Zhao Jingang, Low-temperature molten salt synthesis and characterization of $CoWO_4$ nano-particles, Materials Science and Engineering B 163 (2009) 62–65.

[12] Somchai Thongtem, Surangkana Wannapop, Titipun Thongtem, Characterization of $CoWO_4$ nano-particles produced using the spray pyrolysis, Ceramics International 35 (2009) 2087–2091.

[13] Yu-Xue Zhou, Hong-Bin Yao, Qiao Zhang, Jun-Yan Gong, Shu-Juan Liu, Shu-Hong Yu, Hierarchical $FeWO_4$ microcrystals: solvothermal synthesis and their photocatalytic and magnetic properties, Inorganic Chemistry 48 (2009) 1082–1090.

[14] Q.I. Hui, Jian-feng Huang, Li-yun CAO, Jia-yin LI, Jian-peng WU, Influences of reaction time on the morphology and optical property of CuS microcrystallites prepared by microwave hydrothermal method, Journal of Synthetic Crystals 40 (2011) 1188–1193 (in Chinese).

[15] Shu-hong Yu, Biao Liu, Mao-song Mo, Jian-Hua Huang, Xian-Ming Liu, Yi-Tai Qian, General synthesis of single-crystal tungstate nanorods/nanowires: a facial, low-temperature solution approach, Advanced Materials 13 (2003) 639–647.

[16] Jian Zhang, Yan Zhang, Jing-Yi Yan, Shi-Kuo Li, Hai-Sheng Wang, Fang-Zhi Huang, Yu-Hua Shen, An-Jian Xie, A novel synthesis of star-like $FeWO_4$ nanocrystals via a biomolecule-assisted route, Journal of Nanoparticle Research 14 (2012) 796.

[17] Titipun Thongtem, Anukorn Phuruangrat, Somchai Thongtem, Microwave-assisted synthesis and characterization of $SrMoO_4$ and $SrWO_4$ nanocrystals, Journal of Nanoparticle Research 12 (2010) 2287–2294.